Available online at www.sciencedirect.com

ScienceDirect

Geochimica et Cosmochimica Acta 299 (2021) 1–14

Geochimica et Cosmochimica Acta

www.elsevier.com/locate/gca

Alpha-decay induced shortening of fission tracks simulated by in situ ion irradiation

Weixing Li [a,*], Yuanyuan Cheng [a,b], Lei Feng [a,c], Jingjing Niu [a], Yingxin Liu [b], Vladimir A. Skuratov [d,e,f], Maxim V. Zdorovets [g,h,i], Lynn A. Boatner [j], Rodney C. Ewing [k,*]

[a] *CAS Centre for Excellence in Tibetan Plateau Earth Sciences, and Key Laboratory of Continental Collision and Plateau Uplift, Institute of Tibetan Plateau Research, Chinese Academy of Sciences, Beijing 100101, China*
[b] *School of Gemology, China University of Geosciences, Beijing 100083, China*
[c] *School of Earth Sciences, Lanzhou University, Lanzhou 730000, China*
[d] *Flerov Laboratory for Nuclear Reactions, Joint Institute for Nuclear Research, Dubna, Russia*
[e] *National Research Nuclear University MEPhI, Moscow, Russia*
[f] *Dubna State University, Dubna, Moscow Region, Russia*
[g] *The Institute of Nuclear Physics of the Republic of Kazakhstan, Nur-Sultan, Kazakhstan*
[h] *L.N. Gumilyov Eurasian National University, Nur-Sultan, Kazakhstan*
[i] *Ural Federal University, Yekaterinburg, Russia*
[j] *Materials Science & Technology Division, Retired, Oak Ridge National Laboratory, P.O. Box 2008, Oak Ridge, TN 37831-6044, USA*
[k] *Department of Geological Sciences, Stanford University, Stanford, CA 94305-2115, USA*

Received 13 August 2020; accepted in revised form 20 January 2021; available online 3 February 2021

Abstract

The diffusion of defects (e.g., vacancies and interstitials) and elements used for dating (e.g., He and Pb) in a mineral structure is a thermal process: This is the primary assumption used to determine the age and thermal history of minerals. For instance, thermal history reconstruction, through the number and length distribution of tracks produced by spontaneous fission of ^{238}U, is obtained by assuming a thermal event to be the only energy source for shortening of fission tracks. Here, we report a new, non-thermal energy source that induces additional shortening of fission tracks by the irradiation of alpha-recoils from the alpha-decay of ^{238}U and ^{232}Th. We simulate alpha-decay induced track-shortening by combining ion accelerator irradiations with transmission electron microscopy. This allows for the first observation of track-shrinkage during *in situ* ion irradiation. We show that rather than alpha-particles, alpha-recoils induce a significant shortening of fission tracks by nuclear-collisions. The shortening of track-length can be quantified as a function of alpha-decay event dose. However, apatite is less sensitive than zircon to this non-thermal process. The findings exemplify the interactions among different types of self-irradiation from alpha-particles, alpha-recoils and fission-fragment nuclei in single mineral grains and have important implications for the use of zircon and apatite for radiometric dating and thermochronology.

Keywords: Zircon; Apatite; Fission tracks; Alpha-decay; Radiation effects

* Corresponding authors.
E-mail addresses: wxli@itpcas.ac.cn (W. Li), rewing1@stanford.edu (R.C. Ewing).

https://doi.org/10.1016/j.gca.2021.01.022
0016-7037/

1. INTRODUCTION

Internal irradiation by alpha-decay and spontaneous fission events creates alpha-recoil damage and fission tracks, respectively. However, radiation may induce the recovery of preexisting radiation damage under certain circumstances. This has a profound impact on the mobility of defects (e.g., vacancies and interstitials) and elements used for dating (e.g., He and Pb) at the atomic-scale (Cherniak et al., 1991; Gleadow et al., 2002; Shuster et al., 2006), thereby influencing the interpretation of the age and thermal history for the geological processes at the Earth's larger scale (Lee et al., 1997; Valley et al., 2014; Kusiak et al., 2015; Gerin et al., 2017; Willett et al., 2017). Ionization-induced annealing of preexisting radiation damage (e.g., alpha-recoil damage) by ions with energies ranging from low energy alpha-particles (Ouchani et al., 1997; Li et al., 2017), intermediate (Zhang et al., 2015) and swift (Benyagoub et al., 2006) energy ions, has been documented in some nuclear materials used for stabilizing and immobilizing radioactive waste. Assuming similar radiation-effects for minerals in nature, interactions between the two types of internal irradiation (or self-irradiation), could potentially lead to alpha-decay induced shortening of fission tracks; thus, track length should also be a function of alpha-decay event dose. However, until now, heat has been used as the only energy source for the recovery of radiation damage in both fission track and (U-Th)/He thermochronology (Laslett et al., 1987; Ketcham, 2005; Shuster and Farley, 2009; Reiners et al., 2017), and thermal histories are reconstructed by combining the distributions of etched track-length with the apparent fission track age (Gleadow et al., 1986; Tagami et al., 1990; Ketcham et al., 1999; Gleadow et al., 2002; Ketcham, 2019).

In apatite [$Ca_5(PO_4)_3(F, Cl, OH)$, $P6_3/m$] from Fennoscandia, alpha-decay induced annealing of fission tracks has been proposed as the cause of the observed younger fission-track ages and shorter mean track-length at higher α-doses (Hendriks and Redfield, 2005, 2006). A similar trend has also been found in apatite from other places (McDannell et al., 2019) and in zircon ($ZrSiO_4$, $I4_1/amd$) (Carter, 1990; Shi et al., 2019), showing younger fission-track ages with increasing U concentration. Lacking experimental evidence, however, this speculation has met intense rebuttals, mainly on the reliability of the observed trend (Green and Duddy, 2006; Larson et al., 2006; Kohn et al., 2009). First, rather than by the self-irradiation from alpha-decay, the distribution of etched track-lengths can be significantly complicated by other factors, e.g., the crystallographic orientations (Green and Durrani, 1977; Donelick, 1991), the varied thermal histories of the samples, and the different production-times of individual fission tracks accumulated over time in a sample. Second, the concentration of Th is often not measured but is required in order to calculate the correct α-doses on existing fission tracks. The contribution of Th to alpha-decay event dose cannot be neglected, especially in minerals with high Th/U ratios.

Fission track thermochronology, often jointly used with the (U-Th)/He or U-Pb methods, has found widespread application in studies of tectonics, landscape evolution and basin analysis (Gallagher et al., 1998; House et al., 2002; Chew et al., 2011; Wang et al., 2012; Karlstrom et al., 2014; Schildgen et al., 2018). However, there have been no studies that have separated the possible fission-track shortening induced by alpha-decay from that induced thermally, despite the importance of this issue.

In this study, we simulate the alpha-decay induced effects on latent, or *unetched*, fission tracks by combining ion beam irradiation with transmission electron microscopy (TEM). This enables the observation of the morphological change of latent ion-tracks during *in situ* irradiations using 1 MeV Kr^{2+} ions (simulating alpha-recoils) or 400 keV He^{+} ions (simulating alpha-particles). In contrast, the gradual change cannot be seen using etched fission tracks, since the latent tracks are fully removed once they are etched. These simulations are implemented in three sequential steps: (*i*) production of parallel tracks created by ions with masses and energies of fission fragments using an accelerator, (*ii*) preparation of 50 nm-thick TEM specimens containing parallel ion-tracks by the diamond-knife cutting method (Li et al., 2012), and (*iii*) subsequent *in situ* TEM observations of track-shrinkage induced by ion-irradiations using another ion beam accelerator that simulates the alpha-decay event effect. The contribution of alpha-recoils to track-shortening has been generally neglected, because alpha-recoils produce rather than recover damage. However, we show that instead of alpha-particles, alpha-recoil nuclei produce even more severe track-shrinkage by nuclear collisions with the track. The shrinkage of fission tracks induced, either thermally or by nuclear-collisions, inhibits chemicals used for etching from advancing along the track, leading to a similar shortening of etchable tracks. More importantly, the present study shows that zircon is more sensitive than apatite to alpha-recoil-induced shortening of fission tracks. In addition, zircon normally experiences much higher α-doses in nature than apatite. Thus, the length-shortening in fission tracks induced by alpha-decay must be considered in zircon but may be neglected in apatite.

2. METHODS

2.1. Ions for simulating self-irradiation

The main sources of self-irradiation in minerals are from alpha-decay events and fission events. An atom of ^{238}U fissions (Murakami et al., 1991; Gleadow et al., 2002) into a pair of heavy fission fragment (e.g., an 80 MeV Xe ion in Fig. 1a) and light fission fragment (e.g., 107 MeV Kr ion in Fig. 1b) traveling in opposite directions and creating a damage trail by electronic excitations, which is approximately 9–13 μm in length in each direction. Therefore, the tracks induced by either 80 MeV Xe or 107 MeV Kr ions can be used to simulate one-half of a fission track. These two types of ions produce no significant differences in the track-diameter, even in different target materials (e.g., apatite and zircon in Fig. 1a, b), since they are similar in electronic energy loss per unit depth, $-(dE/dx)_e$, as a function of target depth. Much more commonly, an atom of ^{238}U

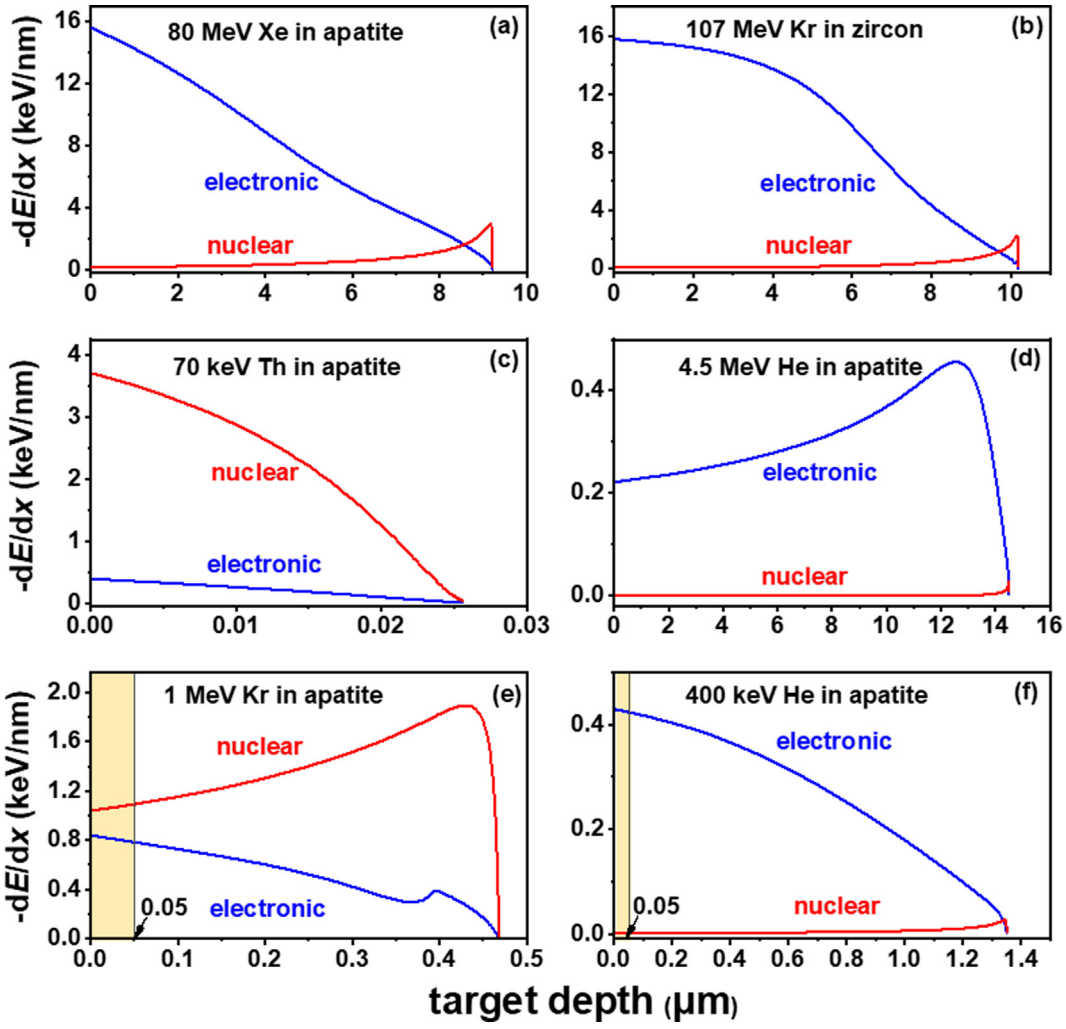

Fig. 1. Electronic and nuclear energy losses, $-\mathrm{d}E/\mathrm{d}x$, as a function of target depth, x, are calculated by SRIM program for the ion-irradiation at different conditions. (a) 80 MeV Xe ions (i.e., simulating heavy fission fragment), (b) 107 MeV Kr ions (simulating light fission fragment), (c) 70 keV Th ions (alpha-recoils), (d) 4.5 MeV He ions (alpha-particles), (e) 1 MeV Kr^{2+} ions (simulating alpha-recoils), and (f) 400 keV He^{+} ions (simulating alpha particles). For the *in situ* TEM ion irradiation experiments (e and f), one must ensure that the incident ions penetrate the sample thickness ~50 nm (marked by orange boxes).

decays into a pair of alpha-recoil (e.g., 70–100 keV Th in Fig. 1c) and alpha-particle (e.g., 4.5 MeV He in Fig. 1d), with an ion-range of ~25 nm and ~14 μm, respectively in opposite directions (Ketcham et al., 2013). The ratio between alpha-decay events and fission events is $\sim 2 \times 10^6$ for ^{238}U and is even higher in the presence of a significant amount of ^{232}Th, providing for a higher dose of alpha-decay events in latent fission-tracks. In order to simulate alpha recoils, the incident ions should be dominated by nuclear collisions, or $-(\mathrm{d}E/\mathrm{d}x)_n$ (Fig. 1c, e), which produces damage (vacancies and displacements). Whereas, for simulating alpha-particles, the incident ions should be dominated by electronic interactions, that is, $-(\mathrm{d}E/\mathrm{d}x)_e$ (Fig. 1d, f), which may induce recovery of alpha-recoil damage in some materials, such as apatite (Li et al., 2017).

In the last two decades, 1 or 1.5 MeV Kr^{2+} ions have been routinely used in *in situ* ion-irradiation experiments to simulate alpha-recoils, since the two energies of Kr^{2+} ions are both dominated by ballistic interactions between the incident ion and the target atoms (Fig. 1c, e) (Wang et al., 1994; Wang et al., 2000; Li et al., 2017). In contrast, typical alpha-recoil nuclei, such as 70 keV Th ions (Fig. 1c), are actually unsuitable for simulating alpha-recoils for *in situ* ion-irradiation due to their insufficient ion ranges, which are needed to penetrate the TEM sample thickness. The dose of Kr ions can be converted into the equivalent dose of alpha-recoils by assuming the same amount of displacements per atom, or dpa, produced by 70 keV Th ions moving along the entire ion range (Fig. 1c) and by 1 MeV Kr^{2+} ions penetrating the sample thickness of 50 nm (Fig. 1e) (Li et al., 2017). For example in apatite, a fluence of 1.0×10^{14}, 1 MeV Kr^{2+} ions/cm^2, D_{Kr}, in this experiment has an equivalent effect along the sample thickness ~50 nm (Fig. 1e) as that of 1.17×10^{19}, alpha-recoils/cm^3 (or 3.66×10^{18} α/g), D_α, in nature (Fig. 1c) using the equation $D_\alpha = D_{Kr}(n_{Kr}/n_\alpha)$, where $n_{Kr} = 0.83$

displacements/(ion.Å), and $n_\alpha = 715$ displacements/α can be estimated by the simulation program SRIM (Ziegler et al., 2010). In zircon, for the same Kr ion-fluence, the equivalent dose is 1.35×10^{19} alpha-recoils/cm^3 (or 2.87×10^{18} α/g), where $n_{Kr} = 1.10$ displacements/(ion.Å), and $n_\alpha = 817$ displacements/α.

The 400 keV He^+ ions have also been routinely used to simulate alpha-particles since they both dissipate most of their energy by electronic excitations (Ewing et al., 2003; Li et al., 2017). Despite having a lower energy than alpha-particles, 400 keV He^+ ions can penetrate the TEM sample thickness of approximately 50 nm in apatite, with an electronic stopping power that is similar to that of alpha-particles (Fig. 1d, f) (Li et al., 2017). A fluence of 1×10^{16}, 400 keV He^+/cm^2, D_{He}, has an equivalent effect along the sample thickness ~50 nm as that of a naturally-occurring dose, D_α, $\sim 1 \times 10^{19}$ α/cm^3 (or 3.13×10^{18} α/g) along the entire length $L_{He} = 14$ μm of the 4.5 MeV alpha particle track, that is, $D_{He} \cong 0.7 D_\alpha L_{He}$, by assuming that the He^+-ion-irradiations in this experiment and the alpha-particles in nature produce the same average fraction of electronic energy-loss-affected volume (Li et al., 2017).

As each alpha-decay event produces an alpha-particle and an alpha-recoil nucleus, the doses of alpha-particles and alpha-recoils are the same. Thus, we can use the above two equations to establish an important connection among alpha-particles, alpha-recoils, 400 keV He^+ ions, and 1 MeV Kr^{2+} ions in order to compare their corresponding radiation-induced effects in both the experiments and in nature.

2.2. The three-step experiments

Fission tracks were simulated by producing parallel ion-tracks in apatite and zircon with ions having typical masses and energies of fission fragment. Two single crystals, i.e., a Durango fluorapatite (density: 3.2 g/cm^3) and a flux-method-synthesized zircon (density: 4.7 g/cm^3) (Zhang et al., 2008), were used in order to see if the alpha-decay induced response of fission tracks depends on the target material. High-quality single-crystals, with a size larger than ~3 mm, are necessary for the very delicate microtome cutting in the next step. However, natural zircon samples are usually too brittle due to their having many fractures and voids. Synthesis of high-quality large fluorapatite single crystals is unnecessary as such large (size: 5–8 mm) high-quality single-crystals are easy to obtain in Durango apatite. In apatite, 80 MeV Xe ions were used at the Cyclotron DC-60 at the National Nuclear Centre in Kazakhstan to produce ion-tracks along the *c* axis of 200 μm-thick-slices of apatite, after heating at 500 °C for 5 h to fully remove the pre-existing alpha-recoil damage and fission tracks. As the density of fission tracks in natural apatite is too low (~10^6 tracks/cm^2) to be observed by TEM, a much higher density (5×10^{10} ions/cm^2) of ion-tracks was produced and used in this work. At the same time, this track density is low enough not to influence the behavior of the materials. In the case of zircon, ion-tracks were created along the *c* axis of 200 μm-thick-slices of zircon by 107 MeV Kr ions using a fluence of 5×10^{10} ions/cm^2 at the IC-100 cyclotron at the Flerov Lab. of Nuclear Reactions in Dubna, Russia.

Cross-sectional TEM specimens containing parallel ion-tracks were prepared by cutting the 80 MeV Xe ion- or 107 MeV Kr ion-irradiated sample along the ion paths with a diamond knife by the microtome cutting method (Li et al., 2012). As track-radius *R* decreases with decreasing electronic stopping power along the incident ions (Fig. 1a, b), tracks with different diameters were obtained in TEM sectioned slices from different target depths, *x*. This method also ensures that all the ion-tracks are parallel to the *c*-axis of apatite and zircon, and all the TEM sections have a uniform sample thickness and identical crystallographic orientation. The irradiated specimens were thinned to a thickness slightly greater than 10 μm for apatite, and ~30 μm for zircon, by mechanical polishing the unirradiated surface. A thin layer of gold ~20 nm was deposited on the irradiated surface as a "surface marker" before the specimen was polished and then mounted in the microtome. The automatic advance of the mounted specimen, ~50 nm for each cut, controlled the thickness of the sectioned slices that were floated on distilled water before being loaded onto a carbon thin-film TEM grid.

The alpha-decay induced shrinkage of fission tracks was simulated by *in situ* irradiations of 1 MeV Kr^{2+} ions or 400 keV He^+ ions. Thermal annealing takes place at room temperature in hours or days immediately after the formation of fission tracks, but no additional reduction of track-length can be measured at room temperature after one month (Donelick et al., 1990; Tamer and Ketcham, 2020). Thus, the chance of room-temperature thermal-annealing was low in this study, as at least 3 years passed between track creation and TEM observation. This ensures that the fission-track shortening induced by alpha-decay can be separated from that induced thermally by using ion-irradiation experiments at room temperature. The morphological change of the ion-tracks was directly recorded at room temperature or 150 °C using a TEM connected to the beam line of the IVEM Tandem Facility at the Argonne National Laboratory. A hot-stage TEM specimen holder was used to heat the ion-tracks during the ion-irradiations. Since the temperature at the specimen holder tip was monitored by a hot-stage controller, it was maintained near the temperature of the specimen stage. The ion beam was incident at 30° from the microscope optic axis and electron beam. This setting assured that the ion beam was perpendicular to the specimen during the ion irradiations, and at the same time it allowed for imaging the morphologies of the specimen in the interval of the ion irradiations by tilting 30° back to align the specimen perpendicular to the electron beams. Ion dosimetry was monitored using Faraday cups within the microscope and 2 cm from the sample. The flux (or fluence rate) for the ion irradiations of 1 MeV Kr^{2+} and 400 keV He^+ was approximately 2.50×10^{11} Kr^{2+} ions/cm^2/s and 6.25×10^{11} He^+ ions/cm^2/s, respectively. These fluxes are low enough to avoid any thermal effect on the irradiated specimens. During each interval of ion-irradiation, the time required to take a TEM image of the ion-tracks of interest was minimized to ~1 s, and the electron-beam current was kept as low as possible (0.1–1 A/cm^2) to minimize the electron-beam induced damage on the ion-tracks. The *in situ* TEM

has the advantage of maintaining the image settings, such as the focus conditions and the beam size (Paul and Fitzgerald, 1992). This greatly minimizes the errors in the measurements of the track-diameter.

3. RESULTS

3.1. The 1 MeV Kr^{2+} ion irradiation of apatite tracks at room temperature

The morphological changes (e.g., local track radius) of parallel 80 MeV Xe ion-induced tracks in apatite were recorded at room temperature (RT) during *in situ* TEM ion-irradiations with 1 MeV Kr^{2+} ions to simulate the alpha-recoil (e.g., 70 keV Th) induced shrinkage of fission tracks. The irradiation properties of these ions are detailed in Fig. 1. The track-profile of 80 MeV Xe ions in apatite was previously obtained by measuring the track-diameter, d, at each location along the entire track length (or the distance to the irradiated surface), x, up to 8.7 μm (Li et al., 2012). Thus, three TEM sections containing parallel tracks with initial mean track-diameters: 8.9, 5.2, and 2.7 nm, were selected to represent one half of a fission-track at a distance, $x = 0$, 4.8 and 7.0 μm, respectively, from the irradiated surface.

The gradual shrinkage of unetched ion-tracks is evident by visually comparing the change of track-size as the ion-irradiation fluence increases from 0 to 9.4×10^{14} Kr^{2+}/cm^2. For each initial diameter, four representative images, selected from up to 16 ion fluences, of the ion-tracks before and at each of the three intervals of ion-irradiations are shown in Fig. 2. The tracks with a smaller mean diameter (e.g., 2.7 nm in Fig. 2i–l) shrink at a faster rate than the wider tracks (e.g., 5.2 nm in Fig. 2e–h and 8.9 nm Fig. 2a–d), similar to the faster fading rate of smaller latent fission tracks upon heat treatment - as observed by *in situ* thermal annealing experiments (Li et al., 2012). However, track-shrinkage cannot be visually observed at the lowest fluence 3.1×10^{12} Kr^{2+} ions/cm^2. The track shrinkage is not evident until $\sim 6.3 \times 10^{13}$ Kr^{2+}/cm^2 (see the relatively smaller tracks in Fig. 2f, j), or the equivalent of 2.3×10^{18} alpha-recoils/g. See dose-conversion in Methods. Thus, this fluence (or dose) can be considered as the critical fluence at which the track-shrinkage is first apparent. Note that in natural apatite, the typical dose for tectonically active area is between 10^{15} and 10^{16} α/g (Gleadow et al., 2002), and up to 2.7×10^{17} α/g for deep time thermochronology (Danisik et al., 2010; Recanati et al., 2017; Ault et al., 2019). The *in situ* Kr^{2+} ion irradiation experiment suggests that in nature such alpha-recoil induced shrinkage of fission tracks is not significant even when the alpha-dose reaches a very high value, e.g., 1×10^{18} α/g (see a more quantitative analysis in Discussion).

3.2. The 400 keV He^+ ion irradiation of apatite tracks at room temperature

The morphology of parallel 80 MeV Xe ion-induced tracks in apatite was recorded by TEM during *in situ* irradiations of 400 keV He^+ ions at room temperature in order to compare the alpha-particle (e.g., 4.5 MeV He ions, Fig. 1) induced shrinkage of fission tracks with the shrinkage induced by alpha-recoil nuclei. No distinct shrinkage, or morphological change in the ion-track can be detected at relatively low He^+ ion fluences equal to or below 8.8×10^{15} He^+/cm^2 (Fig. 3a–c), or equivalent to 2.8×10^{18} alpha-particles/g (see dose conversion in Methods) for tracks with an initial mean diameter of 3.45 nm at a target depth ~6.5 μm from the irradiated surface. When the He^+ ion-fluence reaches the highest value of 2.0×10^{16} He^+/cm^2 (or equivalent to 6.4×10^{18} alpha-particles/g in Fig. 3d) after more than 8 hours of ion-irradiation within the TEM, the shrinkage of ion-tracks is still insignificant, except that now additional "gaps" can be found in some ion-tracks. In contrast, significant shrinkage due to Kr^{2+} ion irradiation is evident at 6.3×10^{13} Kr^{2+}/cm^2 (equivalent to 2.3×10^{18} alpha-recoils/g, see Fig. 2i–j, e–f) for tracks with similar track-diameters. This suggests that the morphological change produced by alpha-recoils is more significant than that caused by alpha-particles. As the alpha-decay event doses are seldom above 2.7×10^{17} alpha/g in apatite (Recanati et al., 2017), the He^+ ion irradiation experiment indicates that the alpha-particle-induced track annealing can be neglected in apatite.

In the target material, no morphological change can be seen during the He^+ ion irradiations up to a fluence of 2.0×10^{16}, 400 keV He^+/cm^2 (Fig. 3d). The damage produced by both 400 keV and 4.5 MeV He^+ ions is insignificant since their major energy loss occurs by electronic interactions (Fig. 1). This is significantly different from the gradual amorphization of the target material upon the nuclear collisions by 1 MeV Kr^{2+} (Fig. 2), as evidenced by the initial formation of separate "mottled" regions between fluences of $0–2.5 \times 10^{14}$ Kr^{2+} ions/cm^2 (yellow arrows in Fig. 2k-l).

3.3. The 1 MeV Kr^{2+} ion irradiation of apatite tracks at 150 °C

In order to investigate whether elevated temperature influences the alpha-recoil induced shrinkage of fission tracks, the morphology of parallel 80 MeV Xe ion-induced tracks in apatite was recorded by TEM during *in situ* irradiations of 1 MeV Kr^{2+} ions at 150 °C. At this temperature, the thermally-induced recovery of ballistic-impact-induced damage in fluorapatite becomes effective but is still lower than the production of damage from the ballistic impacts of the ion-irradiation because previous experiments have indicated that above a critical amorphization temperature, ~200 °C, fluorapatite cannot be fully damaged and remains crystalline (Wang et al., 1994). The elevated temperature (150 °C) was too low to produce any detectable thermal-annealing effect of latent fission tracks in less than 20 minutes during this experiment. In contrast, it takes millions of years for an obvious change to occur in the fission tracks heated at 60–110 °C in nature (Green et al., 1986; Crowley et al., 1991; Carlson et al., 1999; Gleadow et al., 2002; Gleadow and Seiler, 2015).

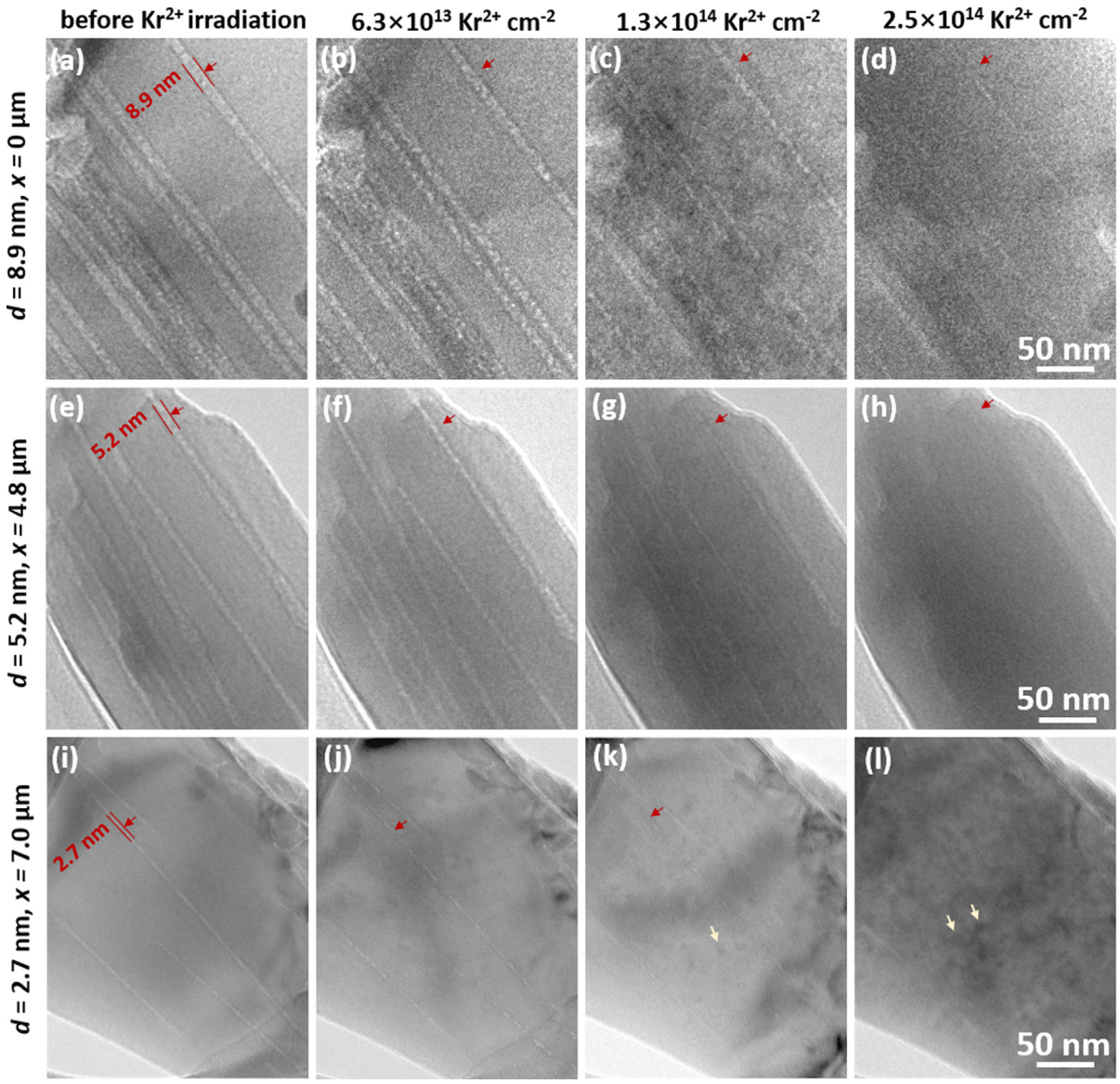

Fig. 2. TEM images show *in situ* 1 MeV Kr^{2+} ions (simulating alpha-recoils) induced gradual shrinkage of parallel tracks produced by 80 MeV Xe ions (simulating fission tracks) in apatite at room temperature. The tracks (red arrows) in each of the three apatite sectioned slices have a similar initial mean track-diameter d (two red parallel lines). As shown at four different representative fluences, the wider ion-tracks, e.g., with (a–d) a diameter of $d = 8.9$ nm, shrink at an obviously slower rate than the smaller tracks, e.g., with (e–h) $d = 5.2$ nm, and (i-l) $d = 2.7$ nm. The track-shrinkage is first apparent (f, j) at $\sim 6.3 \times 10^{13}$ Kr^{2+}/cm^2, or equivalent to 2.3×10^{18} alpha-recoils/g. (For interpretation of the references to colour in this figure legend, the reader is referred to the web version of this article.)

Here we show that ion-tracks shrink at a significantly slower rate at 150 °C than those at room temperature. For example, at the same fluence of 2.5×10^{14} Kr^{2+}/cm^2, an ion-track with initial diameter 8.9 nm shrinks into a line of broken "droplets" at room temperature (Fig. 2a–d); whereas, ion-tracks with the same initial diameter are still continuous at 150 °C despite the obvious shrinkage in track-diameter (Fig. S1a–c in the Supplementary Material). Similar to the room temperature case, tracks with the smaller diameter ~3.5 nm (Fig. S1d–f) shrink much faster than those with larger diameters, e.g., ~8.9 nm (Fig. S1a–c) at 150 °C. However, at the elevated temperature of 150 °C, no morphological changes can be seen in the target material during the Kr^{2+}-ion irradiations up to a fluence of 2.5×10^{14} Kr^{2+}/cm^2 (Fig. S1), which is different from the severe radiation-induced damage at room temperature (Fig. 2). This is consistent with previous results, showing that the accumulation of radiation damage is hindered by the enhanced thermal recovery (Wang et al., 1994).

3.4. The 1 MeV Kr^{2+} ion irradiations of zircon tracks at room temperature

The morphological change of parallel 107 MeV Kr ion-induced tracks in zircon was recorded by TEM during *in situ* irradiations of 1 MeV Kr^{2+} ions at room temperature

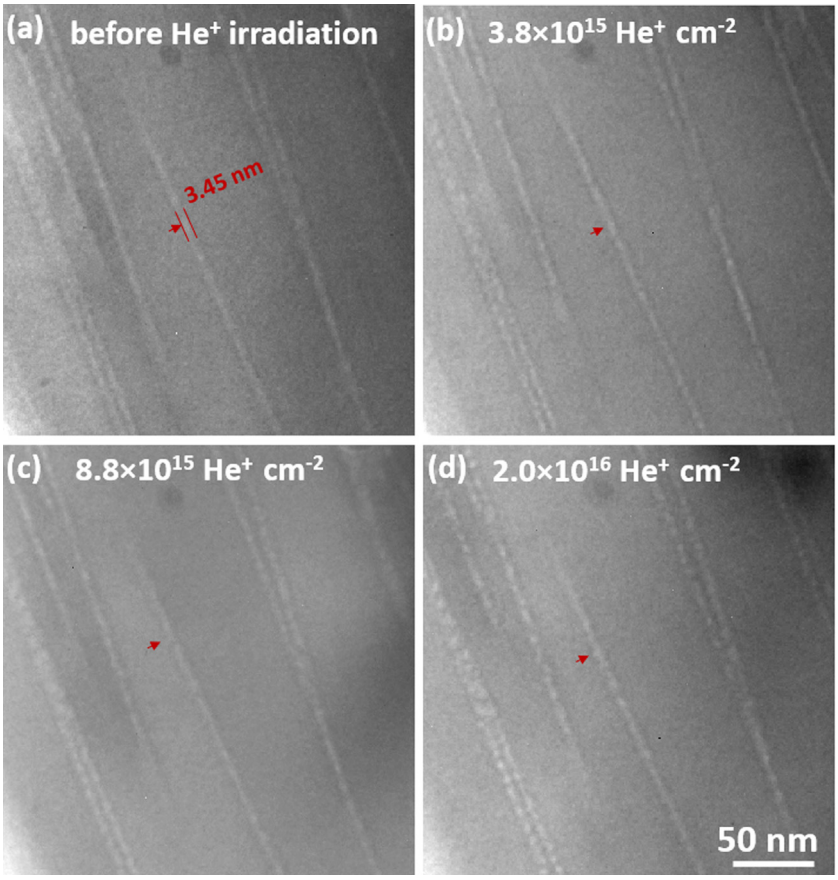

Fig. 3. TEM images show *in situ* 400 keV He^{+} ion-irradiation (simulating α-particles) on the parallel tracks (marked by red arrows) pre-produced by 80 MeV Xe ions in apatite at room temperature. (a–d) No significant shrinkage can be observed at a fluence up to 2.0×10^{16} He^{+}/cm^{2}, or equivalent to 6.4×10^{18} alpha-particles/g. The initial diameter $d = 3.45$ nm of the tracks is marked by two red parallel lines.

to determine whether the alpha-recoil-induced shrinkage of fission tracks depends on the target material. Parallel ion-tracks with an initial mean diameter of 2.85 nm were imaged at a target depth around 6 μm from the irradiated surface. In fact, 107 MeV Kr and 80 MeV Xe ions are similar in electronic energy loss, $-dE/dx$ as a function of target depth (Fig. 1). For a given material, the track-annealing rate depends on the track diameter (or the corresponding electronic $-dE/dx$). Thus, the use of either 107 MeV Kr ions or 80 MeV Xe ions would not cause a difference in the track-annealing rate when similar track-diameters are examined. At an under-focused condition, the amorphous tracks, which have a smaller difference in internal potential with the matrix material zircon, appear dark (Fig. 4) and are significantly different from the bright track-core and dark fringe noted for the highly porous tracks in apatite (Fig. 2) (Li et al., 2011).

The striking difference between zircon and apatite is the much faster rate of 1 MeV Kr^{2+} ion- induced shrinkage of the ion-tracks of zircon (Fig. 4, and Fig. S2 in the Supplementary Material). For example, significant shrinkage can be found in the ion-tracks ($d = 2.85$ nm) of zircon at room temperature at a relatively low fluence of 6.3×10^{12} Kr^{2+}/cm^{2} (Fig. 4a, b), equivalent to 1.8×10^{17} alpha-recoils/g (see the dose conversion for zircon in Methods). Such a low fluence indicates that the alpha-recoil-induced shrinkage of fission tracks in zircon in nature can be significant since zircon has a wider range of alpha-decay event doses, between 10^{17} and 10^{19} α/g, due to the high U and Th concentrations (up to several thousand ppm) (Murakami et al., 1991), and the wide range of ages (up to 4.4 Ga) (Valley et al., 2014). When the fluence reaches $\sim 6.3 \times 10^{13}$ Kr^{2+}/cm^{2} for zircon (Fig. 4d), both the ion-tracks and the surrounding material are highly damaged by the nuclear collisions of the low-energy heavy-ions, and the contrast of ion-tracks is weaker. In addition, the fully amorphous state of the target material is reached at 3.1×10^{14} Kr^{2+}/cm^{2} (Fig. 4f). At this fluence, the contrast of the target-material image becomes very weak, the diffraction rings are diffuse in the inset of diffraction pattern, and no diffraction spots from the zircon are present - all properties consistent with the complete loss of crystallinity.

4. DISCUSSION

4.1. Quantification of nuclear-collision-induced track-shrinkage in apatite

A more quantitative analysis is used to investigate the shrinkage of ion-tracks with different mean diameters by measuring the volume change of tracks during the irradiation of 1 MeV Kr^{2+} ions in apatite (Fig. 5, and Table S1).

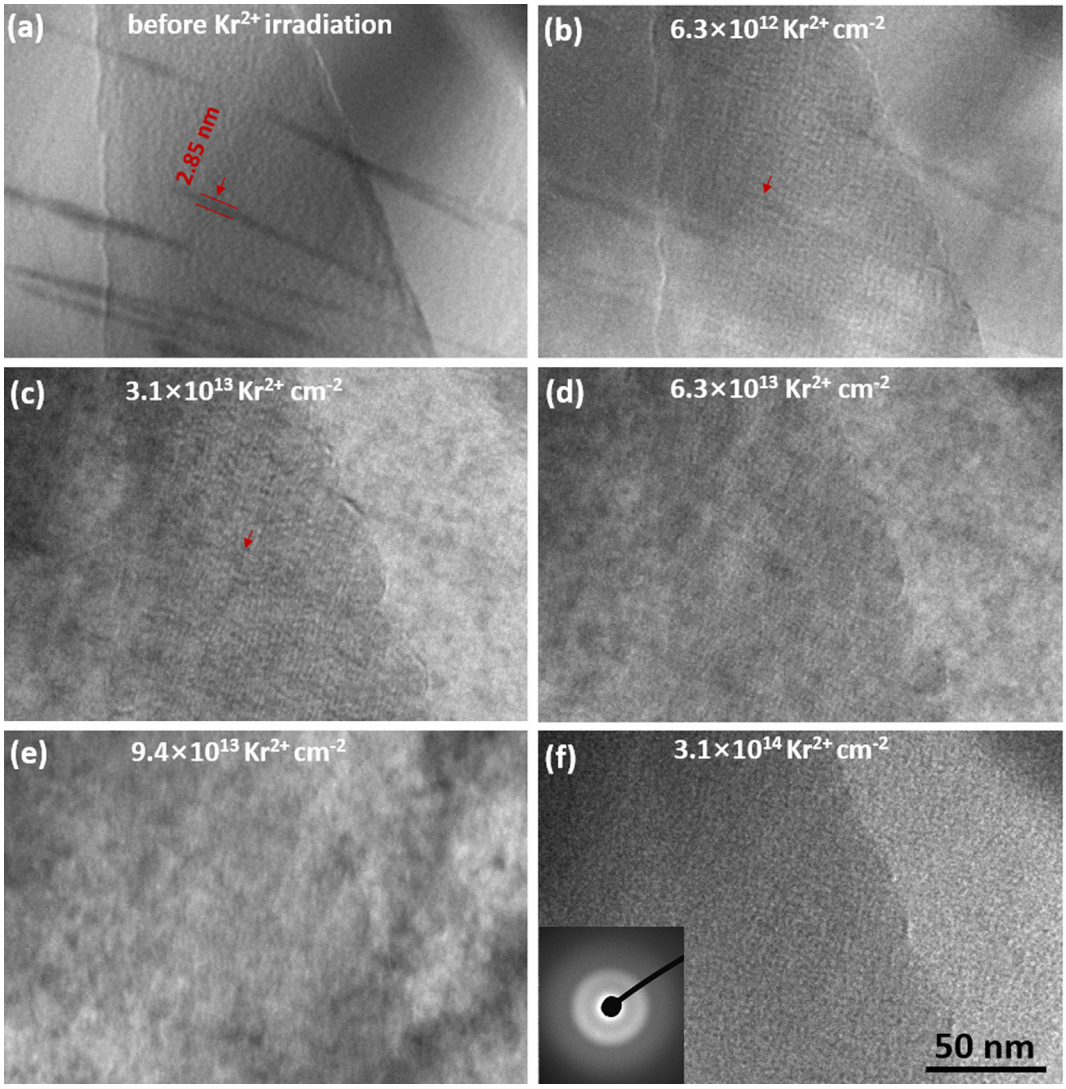

Fig. 4. TEM images showing 1 MeV Kr^{2+} ion-induced gradual shrinkage of parallel 107 MeV Kr ion-tracks (marked by red arrows) with an initial mean diameter of 2.85 nm (marked by two red lines) in zircon at room temperature (a) before, and (b-f) during the irradiation of 1 MeV Kr^{2+} ions. When compared at a similar 1 MeV Kr^{2+} ion fluence and a similar track-diameter, tracks in zircon shrink at a more rapid rate than tracks in apatite (refer to Fig. 2).

For each mean track-diameter (e.g., 8.9, 5.2 and 2.7 nm, taken at a distance $x = 0$, 4.8 and 7.0 μm, respectively, from the irradiated surface), two or three tracks, which should have a sharp contrast with the background and a uniform track-diameter along the length, ~100–400 nm, are selected in order to measure the local track-volume, v, at the same locations (i.e., the distances, x) of these tracks as a function of ion fluence. Rather than the volume of the entire tracks, only the local mean track-diameter, d, and the local mean length, L, can be measured by TEM because of the limited field view and the varied annealing-rates at different places along the entire track. The local track-volume is estimated using $v = \pi d^2 L/4$. The decrease in local track-volume, due to the formation of obvious gaps or track-segmentation for the severely damaged tracks, is subtracted from the volume estimated by the above equation.

The normalized volume as a function of Kr^{2+} ion-fluence for any mean track-diameter can be fit by an equation,

$$v/v_0 = \exp(-BD_{Kr}/T), \quad (1)$$

where v_0 is the initial track-volume, T is sample thickness of 50 nm, and D_{Kr} is ion fluence (ions/cm^2), or equivalent alpha-recoil dose, in α/g (or α/cm^3). The only unknown parameter, i.e., the shrinkage parameter B (in cm^3/ion), can be obtained by fitting. The normalized volume of ion-tracks decreases as the ion-fluence increases. Consistent with the visual observations, the shrinkage parameter increases from 2.4×10^{-20} cm^3/ion for the largest tracks ($d = 8.9$ nm) near the irradiated surface ($x = 0$ μm), to 4.6×10^{-20} cm^3/ion for the medium tracks ($d = 5.2$ nm), and to 7.9×10^{-20} cm^3/ion for the small tracks

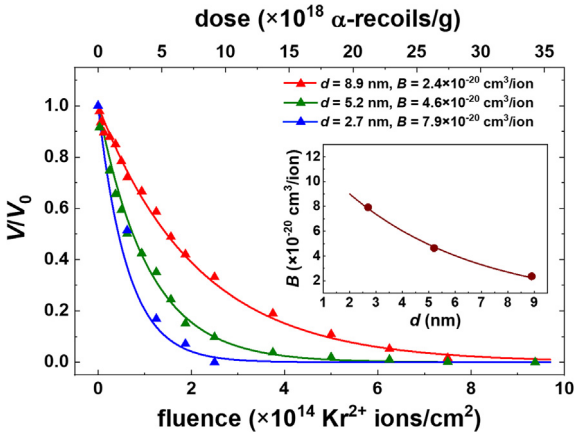

Fig. 5. The normalized volume of ion-tracks in apatite decreases with increasing 1 MeV Kr^{2+} ion-fluence (or equivalent alpha-recoil dose). The normalized volume of 80 MeV Xe ion-induced tracks as a function of fluence of 1 MeV Kr^{2+} (triangles) can be fitted by an equation (solid lines), $v/v_0 = \exp(-BD_{Kr}/T)$. Tracks with a wider diameter, shrink at a slower rate, or have a smaller constant B that can be obtained from the fit. The B values for any other track-diameter can be deduced by fitting the B values of the three measured diameters, e.g., 8.9, 5.2 and 2.7 nm (inset).

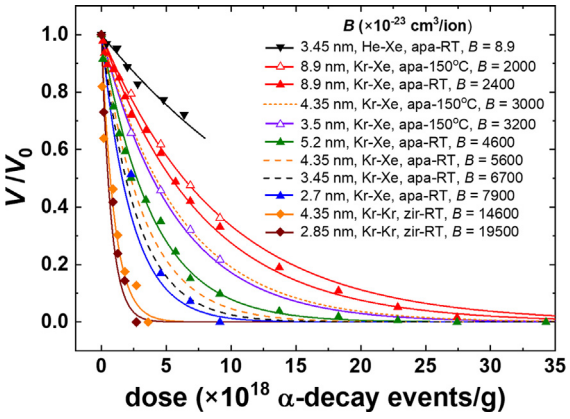

Fig. 6. The shrinkage-rates of ion-tracks for various conditions are compared using a single physical parameter B. By fitting the normalized volume of ion tracks as a function of ion-fluence with the same equation, $v/v_0 = \exp(-BD_{Kr}/T)$, for different combinations (see symbol legends) of (*i*) track-diameter (in nm), (*ii*) ion-types for *in situ* ion-irradiation (1 MeV Kr^{2+} or 400 keV He^{+}) and production of ion-tracks (80 MeV Xe or 107 MeV Kr), and (*iii*) target material and irradiation temperature, the corresponding B value ($\times 10^{-23}$ cm^3/ion) can be obtained. For the convenience of the comparison, the fluences of He^{+} and Kr^{2+} ions have been converted into the equivalent alpha-decay event dose, and three calculated short-dashed or dashed lines have been added.

($d = 2.7$ nm) near the track-end ($x = 7.0$ μm). As the above data are obtained from the three representative locations along the track (see inset in Fig. 5), the shrinkage parameter at any other location can be estimated by an equation that is fit to the above three B values as a function of d,

$$B = B_0 exp(-ad), \quad (2)$$

where the two fitting parameters B_0 and a are 1.346×10^{-19} cm^3/ion and 0.201 nm^{-1}, respectively.

4.2. Comparison of different types of track-shrinkage

We further quantify and compare the shrinkage rates of ion tracks under varying conditions with different combinations of track diameter, ion-types for *in situ* ion-irradiation and the production of ion-tracks, target-material and irradiation-temperature (Fig. 6, and Table S1). Interestingly, the normalized volume at all the conditions can be fitted with Eq. (1). Despite their difference in the units (i.e., Kr^{2+}/cm^2 *vs.* He^{+}/cm^2), the ion-fluences of Kr^{2+} and He^{+} can be converted into the equivalent alpha-decay event dose, as detailed in Methods. Thus, the shrinkage of fission tracks under varied conditions in nature can be conveniently compared by using the values of B, as obtained from the fit from *in situ* ion-irradiations. For example, similar to the trend found in apatite, wider ion-tracks (orange diamonds in Fig. 6) in zircon have a smaller B value than smaller tracks (wine diamonds in Fig. 6), as during the ion-irradiation the 4.35 nm-wide-tracks (Fig. S2) shrink slower than the 2.85 nm-wide tracks (Fig. 4). In addition to the fitted curves, three calculated curves (short-dashed or dashed lines in Fig. 6) are added for the convenience of comparison. Consistent with the visual observations, the following quantified trends can be found in Fig. 6:

(i) In apatite at room temperature, the B value (e.g., 8.9×10^{-23} cm^3/ion for $d = 3.45$ nm, see black triangles in Fig. 6) of tracks induced by alpha particles is ~2–3 orders of magnitude lower than that induced by alpha-recoils, e.g., 6.7×10^{-20} cm^3/ion (black dashed line), as calculated using Eq. (2) with the same d.

(ii) In apatite, a temperature rise leads to a decrease in the B value of ion-tracks. For example, for the same $d = 4.35$ nm, the value of B (5.6×10^{-20} cm^3/ion) at RT (orange dashed line) decreases to 3.0×10^{-20} cm^3/ion at 150 °C (orange short-dashed line). The B value at RT is calculated using Eq. (2), and that at 150 °C is calculated by a linear interpolation of the two B values, 3.2×10^{-20} cm^3/ion for 3.5 nm (violet open triangles) and 2.0×10^{-20} cm^3/ion for 8.9 nm (red open triangles) at the same temperature.

(iii) Zircon is more sensitive than apatite to alpha-recoil-induced shrinkage of fission tracks at room temperature, e.g., for the same track diameter of 4.35 nm, the B value (14.6×10^{-20} cm^3/ion) for zircon (orange diamond) is distinctly larger than that (5.6×10^{-20} cm^3/ion) for apatite (orange dashed line), as calculated using Eq. (2).

More importantly, without heating the zircon or apatite sample, due to the larger B value, the smaller tracks near the track-end shrink faster than the larger tracks in the middle of a fission track. This indicates an important relation that can be used to quantify alpha-recoil induced shortening of track-length as a function of α-dose.

4.3. Quantification of radiation-induced track-shortening in apatite and zircon

In apatite, we further quantify the self-irradiation-induced shortening of an unetched fission track in order to bridge the connection to the length analysis of etched fission tracks, based on the change of the track profile following the ion-irradiation. In fact, the track-profile, i.e., the track-radius at each position along the entire length of tracks induced by 80 MeV Xe ions - as marked with "before irradiation" in Fig. 7a, can be considered as one quarter of the profile of a latent fission track. The ballistically induced atomic displacements from alpha-recoils cause not only the shrinkage of fission tracks but also the shortening of track-length, since the smaller track-radius inhibits the etching chemicals from advancing along the track. The change of track-profile reflects the process of change for the track-radius at any place along the track at the six, representative ion-fluences, from 0 (i.e., before irradiation) up to 6.3×10^{14} Kr^{2+}/cm^2, selected from up to 16 ion fluences (Fig. 7a, and Table S2). Since the profile of a fission track at 0 Kr^{2+}/cm^2 is known, the corresponding B at any position along the track can be calculated using Eq. (2), and then the corresponding radius R at any fluence and any position can be further calculated by combining Eq. (1) with $R = R_0(v/v_0)^{1/2}$, where R_0 is the radius at 0 Kr^{2+}/cm^2. The calculated radii (solid triangles in Fig. 7a) and the measured radii (the larger open triangles at three representative depths of 0, 4.8, and 7.0 μm) are consistent with one another.

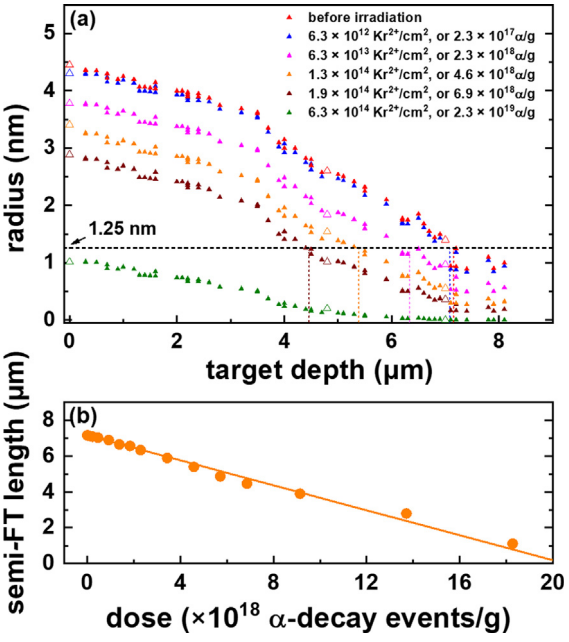

Fig. 7. The radius and etchable length of 80 MeV Xe ion-tracks in apatite shrink with increasing fluence of 1 MeV Kr^{2+} ions or alpha-recoils. (a) The track-profile shows the decreasing radius at each position along the entire length of the ion tracks at the six representative fluences. The radii, marked by the larger open triangles, are measured at the three representative target depths at any fluence. Other radii, marked by the smaller solid triangles at any fluence, are calculated. The etchable lengths of a half of fission track, are obtained at each of α-doses, by assuming that 80 MeV Xe ion-induced tracks cannot be etched until the track-radius is larger than 1.25 nm. (b) The shortening of the etchable length (orange circles) has an approximate linear-relation with increasing α-dose. (For interpretation of the references to colour in this figure legend, the reader is referred to the web version of this article.)

In apatite, the change in the etchable length of fission tracks due to alpha-recoil damage is further estimated by assuming that ion tracks cannot be etched at a target-depth where the track-radius is below a threshold (Fig. 7b, and Table S3). In a previous channeling Rutherford backscattering spectrometry and chemical etching study, four Kr irradiation energies were used to estimate the threshold ≤1.8 nm in apatite (Villa et al., 2000), similar to the thresholds in other oxides (Toulemonde, 1995). In this study, the threshold can be estimated as 1.25 nm, at which the etchable length (or the target depth 7.15 μm) coincides with the contribution of the heavy fission fragment ion (i.e., 80 MeV Xe) to the entire etchable length (16.3 μm) of a neutron-induced fission track (Green et al., 1986; Carlson et al., 1999; Barbarand et al., 2003). As compared to the limited number of irradiation energies (Villa et al., 2000), the track-radius at each place along the entire length of the 80 MeV Xe ion-tracks at 0 Kr^{2+}/cm^2 is obtained from the track profile, which allows for a better estimate of the threshold. Note, that the etchable length is ~2 μm shorter than the range of the heavy fission fragment ions (9–10 μm), as predicted by simulations using SRIM (Ziegler et al., 2010). By intersecting the profiles of ion-tracks with the horizonal line of 1.25 nm at a given depth, the distance from this depth to the irradiated surface ($x = 0$ μm) is obtained as the etchable length, e.g., 7.15, 7.08, 6.33, 5.39 and 4.46 μm at 0, 6.3×10^{12}, 6.3×10^{13}, 1.3×10^{14} and 1.9×10^{14} Kr^{2+}/cm^2, respectively. The shortening of the etchable length, as obtained at the 16 ion fluences, has an approximately linear-relation with increasing α-dose (Fig. 7b). This indicates that in apatite (Fig. 7b), the alpha-recoil-induced track-shortening percentage, $\Delta l/l_0 \times 100\%$, is actually insignificant, where $\Delta l = l_0 - l$, l_0 is the initial etchable length. Even at an extremely high dose in apatite (Danisik et al., 2010; Recanati et al., 2017; Ault et al., 2019), e.g., 2.3×10^{17} α/g (blue triangles), the percentage is merely 0.98%, or equivalent to a shortening of 0.16 μm for a neutron-induced fission track (etchable length:16.3 μm).

In zircon, a similar approach can be used to estimate the track-shortening, but with more assumptions and uncertainties, since a similar profile of fission tracks for zircon is not available (Fig. 8 and Table S3). For simplicity, zircon is assumed to have the same radius (4.45 nm) for a track at the irradiated surface as apatite, and the radius at the end-of-ion range (as simulated by SRIM) is assumed to be zero. Thus, the track-radius, R, at any target depth, x, along a heavy fission fragment ion (e.g., 80 MeV Xe ions) before irradiation, i.e., the track-profile (Fig. 8a), can be assumed to follow a linear relation $R = 5.235 \times 10^{-4}\,x$, where the constant is obtained from the fit of the two coordinate points (0 μm, 4.45 nm) and (8.5 μm, 0 nm). Similarly, the B values for zircon were estimated using Eq. (2), where

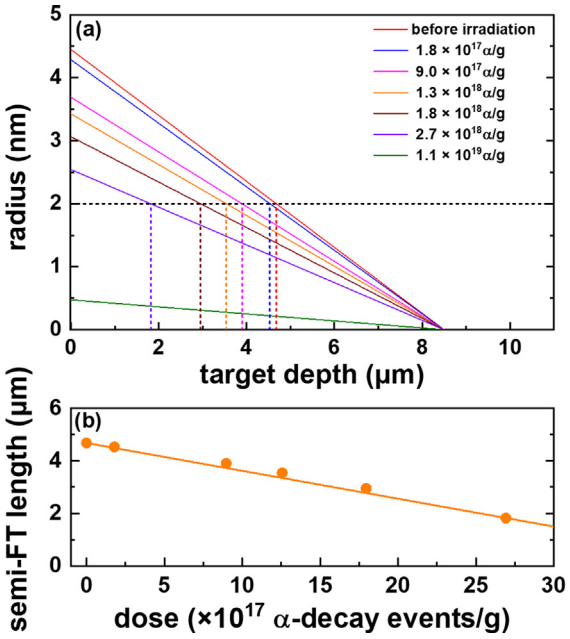

Fig. 8. Track-shortening, as predicted by the calculation of 80 MeV Xe ion-tracks, is significantly faster than that in apatite (refer to Fig. 7), as a result of the larger B and higher α-dose in zircon. (a) The track-profile shows the decreasing radius at each position along the entire length of the 80 MeV Xe ion-induced tracks at the seven fluences. The etchable lengths of a half fission track, are obtained at each of the α-doses, by assuming that 80 MeV Xe ion-induced tracks cannot be etched until the track-radius is larger than 2 nm. (b) The shortening of the etchable length (orange circles) has an approximate linear-relation with increasing α-dose. (For interpretation of the references to colour in this figure legend, the reader is referred to the web version of this article.)

the two parameters B_0 (3.385×10^{-19} cm^3/ion) and a (0.195 nm^{-1}) are obtained by fitting the B values measured at the two diameters (d: 2.85 and 4.35 nm) (navy circles and magenta diamonds in Fig. 6). Similar to the case of apatite, the horizonal line that intersects the track profile at each alpha-dose is set at 2 nm, which ensures the intersected point (4.7 μm, 2 nm) at 0 α/g coincides with the contribution (i.e., $l_0 \cong 4.7$ μm) of the heavy fission fragment ion (i.e., 80 MeV Xe) to the entire etchable length (11 μm) of neutron-induced fission tracks before irradiation (Kasuya and Naeser, 1988; Tagami et al., 1990). The shortening of the etchable length (orange circles in Fig. 8b) in zircon also has an approximately linear relation with increasing alpha-decay event dose. The track-shortening percentages ($\Delta l/l_0 \times 100\%$) due to the self-irradiation of alpha-recoils in zircon are found to be significantly greater than that of apatite: At a very low dose in zircon, for example 1.8×10^{17} α/g (blue line in Fig. 8a), the percentage is ~3.2%; whereas, at a normal dose of 1.3×10^{18} α/g (orange line), it increases to ~24.4%.

As compared to zircon, these effects are less effective for track-shortening in apatite, due to lower alpha-decay event dose and the weaker bonds that are easier to anneal from limited alpha-decay damage. These differences in such radiation-induced effects between apatite and zircon indicate that the younger fission track ages (or shorter track lengths) at high alpha-decay event doses can be more often encountered in zircon than in apatite (Carter, 1990; Hendriks and Redfield, 2005, 2006; McDannell et al., 2019; Shi et al., 2019)

We further infer that thermal events likely lead to additional shortening - preferentially at the gaps where the track-radius is smaller due to the impact of alpha recoils, as the smaller fission tracks segment more easily at higher temperature (Li et al., 2011). Upon the direct impact of an alpha-recoil, a "gap" up to ~2–5 nm (the diameter of alpha-recoil damaged domain) (Murakami et al., 1991; Farnan et al., 2007) can be created on the track. The more rapid shortening of spontaneous fission tracks relative to that of neutron-induced fission tracks at elevated temperatures has been reported previously in zircon (Kasuya and Naeser, 1988). The faster shortening rate has not been explained *via* coupling the radiation-induced gaps in fission tracks with higher temperature. The authors have (Kasuya and Naeser, 1988), however, mentioned that the alpha-recoil damage hinders the etching of surrounding materials. This still cannot explain the experimental result that clearly indicates the gradual increased difference in the etched track length between spontaneous and neutron-induced fission tracks at higher annealing temperatures up to 700 °C (Kasuya and Naeser, 1988), because the thermal treatment would gradually recover the alpha-recoil damage in the sample that contains spontaneous fission tracks. Note, that this track-shortening by coupled radiation and thermal effects should not be confused with the decreased shrinkage rate of ion tracks heated at a relatively low temperature (e.g., 150 °C for apatite in this study) during ion-irradiation due to a thermally-hampered production of damage in the tracks. In the laboratory, a much higher temperature (e.g., 300–400 °C for apatite fission tracks) (Crowley et al., 1991; Gleadow and Seiler, 2015) is required than that occurring in nature to induce observable thermal annealing of fission tracks with gaps; however, this has not been investigated in this study. Currently, the shortening of etchable fission tracks in nature has been attributed to thermal recovery of damaged zones, and this is the basis for the determination of thermal history. More work is required in order to clarify the coupled effects between the damaged fission tracks and higher temperature. In order to improve the precision of thermal history reconstruction, investigators must consider the impact of alpha-recoil damage.

In summary, *in situ* ion irradiation experiments and subsequent quantitative analysis indicate that the shrinkage of the track-volume upon the direct impact of low-energy heavy-ions leads to the shortening of ion-tracks in addition to the well-known thermally induced track-shortening. The shrinkage rate can be quantified and compared by a physical parameter B for tracks under different conditions. The shortening of fission tracks is induced by the direct impact of alpha-recoils, rather than by the alpha-particle-induced damage recovery. In zircon, even at an extremely low fluence, the radiation-induced shortening of etchable track length is significant, thus the non-thermally induced

track-shortening should be considered in zircon. However, this shortening may be neglected in apatite because of the 2–3 times lower *B* value and the much lower dose of alpha-recoils (Gleadow et al., 2002; Danisik et al., 2010; Recanati et al., 2017; Ault et al., 2019).

Declaration of Competing Interest

The authors declare that they have no known competing financial interests or personal relationships that could have appeared to influence the work reported in this paper.

ACKNOWLEDGMENTS

This work is supported by the Strategic Priority Research Program of Chinese Academy of Sciences (XDA20070201), the National Second Expedition to the Tibetan Plateau (2019QZKK0707), and National Natural Science Foundation of China (NSFC 41673062). The electron microscopy with *in situ* ion irradiation was accomplished at Argonne National Laboratory at the IVEM-Tandem Facility, a U.S. Department of Energy Facility funded by the DOE Office of Nuclear Energy, operated under Contract No. DEAC02-06CH11357 by U. Chicago Argonne, LLC. The authors thank warmly M. Kirk, E. Ryan and P. Baldo from Argonne National Laboratory for assistance with the *in situ* TEM experiments. We thank David Shuster and three anonymous reviewers for their suggestions and comments to improve this paper.

APPENDIX A. SUPPLEMENTARY MATERIAL

Supplementary data to this article can be found online at https://doi.org/10.1016/j.gca.2021.01.022.

REFERENCES

Ault A. K., Gautheron C. and King G. E. (2019) Innovations in (U-Th)/He, fission track, and trapped charge thermochronometry with applications to earthquakes, weathering, surface-mantle connections, and the growth and decay of mountains. *Tectonics* **38**, 3705–3739.

Barbarand J., Hurford T. and Carter A. (2003) Variation in apatite fission-track length measurement: implications for thermal history modelling. *Chem. Geol.* **198**, 77–106.

Benyagoub A., Audren A., Thomé L. and Garrido F. (2006) Athermal crystallization induced by electronic excitations in ion-irradiated silicon carbide. *Appl. Phys. Lett.* **89**, 241914.

Carlson W. D., Donelick R. A. and Ketcham R. A. (1999) Variability of apatite fission-track annealing kinetics: I. Experimental results. *Am. Mineral.* **84**, 1213–1223.

Carter A. (1990) The thermal history and annealing effects in zircons from the ordovician of North Wales. *Nucl. Tracks Radiat. Meas.* **17**, 309–313.

Cherniak D. J., Lanford W. A. and Ryerson F. J. (1991) Lead diffusion in apatite and zircon using ion-implantation and Rutherford backscattering techniques. *Geochim. Cosmochim. Acta* **55**, 1663–1673.

Chew D. M., Sylvester P. J. and Tubrett M. N. (2011) U-Pb and Th-Pb dating of apatite by LA-ICPMS. *Chem. Geol.* **280**, 200–216.

Crowley K. D., Cameron M. and Schaefer R. L. (1991) Experimental studies of annealing of etched fission tracks in fluorapatite. *Geochim. Cosmochim. Acta* **55**, 1449–1465.

Danisik M., Pfaff K., Evans N. J., Manoloukos C., Staude S., McDonald B. J. and Markl G. (2010) Tectonothermal history of the Schwarzwald Ore District (Germany): An apatite triple dating approach. *Chem. Geol.* **278**, 58–69.

Donelick R. A. (1991) Crystallographic orientation dependence of mean etchable fission-track length in apatite - an empirical-model and experimental-observations. *Am. Mineral.* **76**, 83–91.

Donelick R. A., Roden M. K., Mooers J. D., Carpente B. S. and Miller D. S. (1990) Etchable length reduction of induced fission tracks in apatite at room temperature (~23°C): crystallographic orientation effects and "initial" mean lengths. *Nucl. Tracks Radiat. Meas.* **17**, 261–265.

Ewing, R.C., Meldrum, A., Wang, L.M., Weber, W.J., Corrales, L. R., 2003. Radiation effects in zircon. In: Hanchar, J.M., Hoskin, P.W.O. (Eds.), Zircon. Rev. Mineral. Geochem., Chantilly, pp. 387–425.

Farnan I., Cho H. and Weber W. J. (2007) Quantification of actinide alpha-radiation damage in minerals and ceramics. *Nature* **445**, 190–193.

Gallagher K., Brown R. and Johnson C. (1998) Fission track analysis and its applications to geological problems. *Annu. Rev. Earth Planet. Sci.* **26**, 519–572.

Gerin C., Gautheron C., Oliviero E., Bachelet C., Djimbi D. M., Seydoux-Guillaume A. M., Tassan-Got L., Sarda P., Roques J. and Garrido F. (2017) Influence of vacancy damage on He diffusion in apatite, investigated at atomic to mineralogical scales. *Geochim. Cosmochim. Acta* **197**, 87–103.

Gleadow A. J. W., Belton D. X., Kohn B. P. and Brown R. W. (2002) Fission track dating of phosphate minerals and the thermochronology of apatite. *Rev. Mineral. Geochem.* **48**, 579–630.

Gleadow A. J. W., Duddy I. R., Green P. F. and Lovering J. F. (1986) Confined fission-track lengths in apatite: A diagnostic tool for thermal history analysis. *Contrib. Mineral. Petrol.* **94**, 405–415.

Gleadow, A.J.W., Seiler, C., 2015. Fission track dating and thermochronology. In: Rink, J.W., Thompson, J.W. (Eds.), Encyclopedia of Scientific Dating Methods, pp. 285–296.

Green P. F. and Duddy I. R. (2006) Interpretation of apatite (U–Th)/He ages and fission track ages from cratons. *Earth Planet. Sci. Lett.* **244**, 541–547.

Green P. F., Duddy I. R., Gleadow A. J. W., Tingate P. R. and Laslett G. M. (1986) Thermal annealing of fission tracks in apatite. 1. A qualitative description. *Chem. Geol.* **59**, 237–253.

Green P. F. and Durrani S. A. (1977) Annealing studies of tracks in crystals. *Nucl. Track Detect.* **1**, 33–39.

Hendriks B. W. H. and Redfield T. F. (2005) Apatite fission track and (U-Th)/He data from Fennoscandia: An example of underestimation of fission track annealing in apatite. *Earth Planet. Sci. Lett.* **236**, 443–458.

Hendriks B. W. H. and Redfield T. F. (2006) Reply to: Comment on "Apatite Fission Track and (U–Th)/He data from Fennoscandia: An example of underestimation of fission track annealing in apatite" by B. W. H. Hendriks and T. F. Redfield. *Earth Planet. Sci. Lett.* **248**, 569–577.

House M. A., Gurnis M., Kamp P. J. J. and Sutherland R. (2002) Uplift in the Fiordland region, New Zealand: implications for incipient subduction. *Science* **297**, 2038–2041.

Karlstrom K. E., Lee J. P., Kelley S. A., Crow R. S., Crossey L. J., Young R. A., Lazear G., Beard L. S., Ricketts J. W., Fox M.

and Shuster D. L. (2014) Formation of the Grand Canyon 5 to 6 million years ago through integration of older palaeocanyons. *Nat. Geosci.* **7**, 239–244.

Kasuya M. and Naeser C. W. (1988) The effect of α-damage on fission-track annealing in zircon. *Nucl. Tracks Radiat. Meas.* **14**, 477–480.

Ketcham R. A. (2005) Forward and inverse modeling of low-temperature thermochronometry data. In *Low-Temperature Thermochronology: Techniques, Interpretations, and Applications* (eds. P. W. Reiners and T. A. Ehlers). Mineralogical Soc Amer, Chantilly, pp. 275–314.

Ketcham R. A. (2019) Fission-track annealing: From geologic observations to thermal history modeling. In *Fission-Track Thermochronology and its Application to Geology* (eds. M. G. Malusà and P. G. Fitzgerald). Springer International Publishing, Cham, pp. 49–75.

Ketcham R. A., Donelick R. A. and Carlson W. D. (1999) Variability of apatite fission-track annealing kinetics: III. Extrapolation to geological time scales. *Am. Mineral.* **84**, 1235–1255.

Ketcham R. A., Guenthner W. R. and Reiners P. W. (2013) Geometric analysis of radiation damage connectivity in zircon, and its implications for helium diffusion. *Am. Mineral.* **98**, 350–360.

Kohn B. P., Lorencak M., Gleadow A. J. W., Kohlmann F., Raza A., Osadetz K. G. and Sorjonen-Ward P. (2009) A reappraisal of low-temperature thermochronology of the eastern Fennoscandia Shield and radiation-enhanced apatite fission-track annealing. In *Thermochronological Methods: From Palaeotemperature Constraints to Landscape Evolution Models* (eds. F. Lisker, B. Ventura and U. A. Glasmacher). Geological Society Special Publications, London, pp. 193–216.

Kusiak M. A., Dunkley D. J., Wirth R., Whitehouse M. J., Wilde S. A. and Marquardt K. (2015) Metallic lead nanospheres discovered in ancient zircons. *Proc. Natl. Acad. Sci. U. S. A., Early Ed.* **112**, 4958–4963.

Larson S. Å., Cederbom C. E., Tullborg E. L. and Stiberg J. P. (2006) Comment on "Apatite fission track and (U–Th)/He data from Fennoscandia: An example of underestimation of fission track annealing in apatite" by Hendriks and Redfield [Earth Planet. Sci. Lett. 236 (443–458)]. *Earth Planet. Sci. Lett.* **248**, 561–568.

Laslett G. M., Green P. F., Duddy I. R. and Gleadow A. J. W. (1987) Thermal annealing of fission tracks in apatite. 2. A quantitative-analysis. *Chem. Geol.* **65**, 1–13.

Lee J. K. W., Williams I. S. and Ellis D. J. (1997) Pb, U and Th diffusion in natural zircon. *Nature* **390**, 159–162.

Li W. X., Lang M., Gleadow A. J. W., Zdorovets M. V. and Ewing R. C. (2012) Thermal annealing of unetched fission tracks in apatite. *Earth Planet. Sci. Lett.* **321–322**, 121–127.

Li W. X., Shen Y. H., Zhou Y. Q., Nan S., Chen C. H. and Ewing R. C. (2017) *In situ* TEM observation of alpha-particle induced annealing of radiation damage in Durango apatite. *Sci. Rep.* **7**, 14108.

Li W. X., Wang L. M., Lang M., Trautmann C. and Ewing R. C. (2011) Thermal annealing mechanisms of latent fission tracks: Apatite vs. zircon. *Earth Planet. Sci. Lett.* **302**, 227–235.

McDannell K. T., Issler D. R. and O'Sullivan P. B. (2019) Radiation-enhanced fission track annealing revisited and consequences for apatite thermochronometry. *Geochim. Cosmochim. Acta* **252**, 213–239.

Murakami T., Chakoumakos B. C., Ewing R. C., Lumpkin G. R. and Weber W. J. (1991) Alpha-decay event damage in zircon. *Am. Mineral.* **76**, 1510–1532.

Ouchani S., Dran J. C. and Chaumont J. (1997) Evidence of ionization annealing upon helium-ion irradiation of pre-damaged fluorapatite. *Nucl. Instrum. Methods Phys. Res. Sect. B* **132**, 447–451.

Paul T. A. and Fitzgerald P. G. (1992) Transmission Electron-Microscopic investigation of fission tracks in fluorapatite. *Am. Mineral.* **77**, 336–344.

Recanati A., Gautheron C., Barbarand J., Missenard Y., Pinna-Jamme R., Tassan-Got L., Carter A., Douville E., Bordier L., Pagel M. and Gallagher K. (2017) Helium trapping in apatite damage: Insights from (U-Th-Sm)/He dating of different granitoid lithologies. *Chem. Geol.* **470**, 116–131.

Reiners P. W., Carlson R. W., Renne P. R., Cooper K. M., Granger D. E., McLean N. M. and Schoene B. (2017) Radiation-damage methods of geochronology and thermochronology. In *Geochronology and Thermochronology*. John Wiley & Sons Ltd, Chichester, pp. 259–289.

Schildgen T. F., van der Beek P. A., Sinclair H. D. and Thiede R. C. (2018) Spatial correlation bias in late-Cenozoic erosion histories derived from thermochronology. *Nature* **559**, 89–93.

Shi G. Z., Soares C. J., Shen C. B., Wang H., Yang C. Q., Liang C. and Liu M. H. (2019) Combined detrital zircon fission track and U-Pb dating of the Late Paleozoic to Early Mesozoic sandstones in the Helanshan, western Ordos fold-thrust belt: Constraints for provenance and exhumation history. *J. Geodyn.* **130**, 57–71.

Shuster D. L. and Farley K. A. (2009) The influence of artificial radiation damage and thermal annealing on helium diffusion kinetics in apatite. *Geochim. Cosmochim. Acta* **73**, 183–196.

Shuster D. L., Flowers R. M. and Farley K. A. (2006) The influence of natural radiation damage on helium diffusion kinetics in apatite. *Earth Planet. Sci. Lett.* **249**, 148–161.

Tagami T., Ito H. and Nishimura S. (1990) Thermal annealing characteristics of spontaneous fission tracks in zircon. *Chem. Geol.* **80**, 159–169.

Tamer M. and Ketcham R. (2020) Is low-temperature fission-track annealing in apatite a thermally controlled process? *Geochem. Geophys. Geosyst.* **21**.

Toulemonde M. (1995) Defect creation by swift heavy-ions - material modifications in the electronic stopping power regime. *Appl. Radiat. Isot.* **46**, 375–381.

Valley J. W., Cavosie A. J., Ushikubo T., Reinhard D. A., Lawrence D. F., Larson D. J., Clifton P. H., Kelly T. F., Wilde S. A., Moser D. E. and Spicuzza M. J. (2014) Hadean age for a post-magma-ocean zircon confirmed by atom-probe tomography. *Nat. Geosci.* **7**, 219–223.

Villa F., Grivet M., Rebetez M., Dubois C., Chambaudet A., Chevarier N., Blondiaux G., Sauvage T. and Toulemonde M. (2000) Damage morphology of Kr ion tracks in apatite: Dependence on thermal annealing. *Nucl. Instrum. Methods Phys. Res. Sect. B* **168**, 72–77.

Wang E., Kirby E., Furlong K. P., van Soest M., Xu G., Shi X., Kamp P. J. J. and Hodges K. V. (2012) Two-phase growth of high topography in eastern Tibet during the Cenozoic. *Nat. Geosci.* **5**, 640–645.

Wang L. M., Cameron M., Weber W. J., Crowley K. D. and Ewing R. C. (1994) *In situ* TEM observation of radiation induced amorphization of crystals with apatite structure. In *Hydroxyapatite and Related Materials* (eds. P. Brown and B. Constantze). CRC Press, pp. 243–249.

Wang S. X., Wang L. M., Ewing R. C. and Kutty K. V. G. (2000) Ion irradiation of rare-earth- and yttrium-titanate-pyrochlores. *Nucl. Instrum. Methods Phys. Res. Sect. B* **169**, 135–140.

Willett C. D., Fox M. and Shuster D. L. (2017) A helium-based model for the effects of radiation damage annealing on helium diffusion kinetics in apatite. *Earth Planet. Sci. Lett.* **477**, 195–204.

Zhang M., Boatner L. A., Salje E. K. H., Honda S. and Ewing R. C. (2008) Pb^{+} irradiation of synthetic zircon ($ZrSiO_4$): Infrared spectroscopic investigation. *Am. Mineral.* **93**, 1418–1423.

Zhang Y. W., Sachan R., Pakarinen O. H., Chisholm M. F., Liu P., Xue H. Z. and Weber W. J. (2015) Ionization-induced annealing of pre-existing defects in silicon carbide. *Nat. Commun.* **6**, 8049.

Ziegler J. F., Ziegler M. D. and Biersack J. P. (2010) SRIM - The stopping and range of ions in matter (2010). *Nucl. Instrum. Methods Phys. Res. Sect. B* **268**, 1818–1823.

Associate editor: David L Shuster